Strain Induced Martensitic Transformation in Austempered Ductile Iron (ADI)

Strain Induced Martensitic Transformation in Austempered Ductile Iron (ADI)

X H Li[1], P Saal[2], W M Gan[3], M Landesberger[2], M Hoelzel[1] and M Hofmann[1*]

[1] *Heinz Maier-Leibnitz Zentrum (MLZ), Technische Universität München, Lichtenbergstr. 1, D-85747 Garching, Germany*
[2] *Institute of metal forming and casting, Technische Universität München, Walther-Meißner-Str. 4, D-85747 Garching, Germany*
[3] *German Engineering Materials Centre at MLZ, Helmholtz-Zentrum Geesthacht, D-85747 Garching, Germany*
**Corresponding author. Tel.:+49 289 14744; fax: +49 89 289 14666*

Keywords:

neutron powder diffraction, retained austenite, phase analysis, texture

Abstract

The strain induced martensitic transformation in austempered ductile iron (ADI) has been investigated using high resolution neutron diffraction on samples compressed ex-situ to different plastic strains. In addition bulk texture measurements using neutron diffraction have been performed to calculate the orientation distribution of ferrite and austenite phases for different strain levels. Combing the detailed texture information with neutron diffraction pattern proved to be essential for quantitative phase analysis and extraction of martensite phase fractions. The martensite content induced by strain in ADI depends on austempering temperature and degree of deformation.

1. Introduction

Austempered ductile iron (ADI) is a nodular ductile iron which has undergone a special heat treatment to enhance mechanical properties to a great extent. The heat treatment process of ADI consists of austenitization followed by quenching to a temperature typically between 250°C and 450°C and isothermal austempering [1]. After such a heat treatment the microstructure of ADI consists of acicular ferrite (α) and high carbon enriched retained austenite (γ). The microstructure strongly depends on the austenitization and austempering temperatures. Details on dependence of microstructure and temperature can be found in [1-6]. In industrial applications alloying elements such as Ni, Mo or Cu are used in order to delay the phase transition kinetics, which improves the austemperability of heavy sections.

The high carbon enriched austenite is metastable and several reports exist indicating a transformation induced plasticity effect (TRIP) when ADI is subjected to deformation [7-9]. During the plastic deformation the high carbon enriched retained austenite can transform to martensite. Austenitization temperature (T_γ), austempering temperature (T_{Aus}), austempering time and alloying

composition can influence the retained austenite fraction, its grain size and stability [3, 4], which in turn will affect the possible martensitic transformation.

The relationship between heat treatment parameters and phase fractions in ADI has been extensively studied by Meier et al. using in-situ neutron powder diffraction on non-textured samples [1]. On the other hand in case of the deformation induced martensitic transformation in ADI quantitative phase analysis is hindered due to texture formation and standard Rietveld analysis fails to produce reliable results. However, the incorporation of texture information into Rietveld refinements to extract quantitative phase information has been already successfully applied in various studies [e.g. 10-12].

A similar approach is therefore used in the current work where the influence of different treatments and composition parameters on the martensitic transformation has been studied using high resolution neutron powder diffraction and texture measurements on samples after compression to different plastic strains. The results from these experiments allow us to relate the martensitic transformation kinetics in ADI with austempering temperature and plastic strains.

2. Experimental

Cylindrical ADI samples which contain 3.6wt% C, 2.8wt%Si and 0.2wt%Mn with dimension of Ø 6mm × 10 mm were prepared using different heat treatment parameters which yield microstructures as shown in table 1 (it should be noted that here the volume fractions relate only to the metallic matrix since the change in nodular graphite fraction during austempering is negligible [1]). T_γ and T_{Aus} where selected according to results published elsewhere [13]. The heat treated ADI samples were compressed to different strain levels ranging from 0% up to 40% with a 10% increment in strain. High resolution neutron powder diffraction data were taken from these samples using the diffractometer SPODI at MLZ [14] within a 2θ range = 10~152° and step width of Δ2θ = 0.05°. The wavelength was set to 1.5483Å using a Ge (551) monochromator.

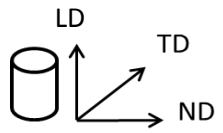

Figure 1. Definition of the sample coordinate system for the pole figures. LD: loading direction; ND: normal direction; TD: transverse direction

Table 1. ADI heat treatment conditions and resulting phase fractions after heat treatment

Austenitization T_γ [°C]	Austempering T_{Aus} [°C]			Austenite [vol%]			Ferrite [vol%]		
900	**400**	**350**	**300**	**40**	**34**	**24**	**60**	**66**	**76**

Complete pole figures of ferrite (110) and (200), austenite (111) and (200) of the ADI samples were measured at the materials science diffactometer STRESS-SPEC [15] with a wavelength of 1.68Å using a Ge (311) monochromator. In the measurements the loading direction (LD) of the samples was perpendicularly to the incoming beam direction (figure 1). The orientation distribution functions of crystallites (ODFs) and then the inverse pole figures were calculated from the measured complete pole figures using the harmonic method [16]. For quantitative phase analysis the program MAUD [11, 12] was used in which texture information via the ODF and Rietveld refinement methods can be combined.

3. Results and discussion

3.1 Texture formation in ADI during plastic deformation

Figure 2a shows high resolution diffraction data on a set of samples which were prepared with the heat treatment parameters T_γ = 900°C/ T_{Aus} = 350°C and then compressed to strain levels of 0%, 20% and 40%, respectively. In case of the unstrained sample the extracted lattice parameters were a = 2.8638(4) Å for ferrite and a = 3.6325(7) Å for austenite. During plastic deformation the carbon enriched retained austenite partly transforms to martensite (at 40% strain: a = 2.880 (2) Å and c = 2.957 (4) Å, c/a-ration = 1.03). The strain induced martensitic transformation is indicated in the diffraction data by a decrease of the austenite peak intensity and an increase of the ferrite peak intensity. The increase in ferrite peak intensity is a consequence of close proximity of ferrite and martensite Bragg reflections, which cannot be separated. Martensite reflections can also be identified as shoulders close to the ferrite peak positions (figure 2b). Extensive peak broadening and overlap of austenite (111), ferrite (110) and martensite (101), (110) reflections make a direct extraction of individual martensite peak intensities difficult using ordinary peak fitting methods.

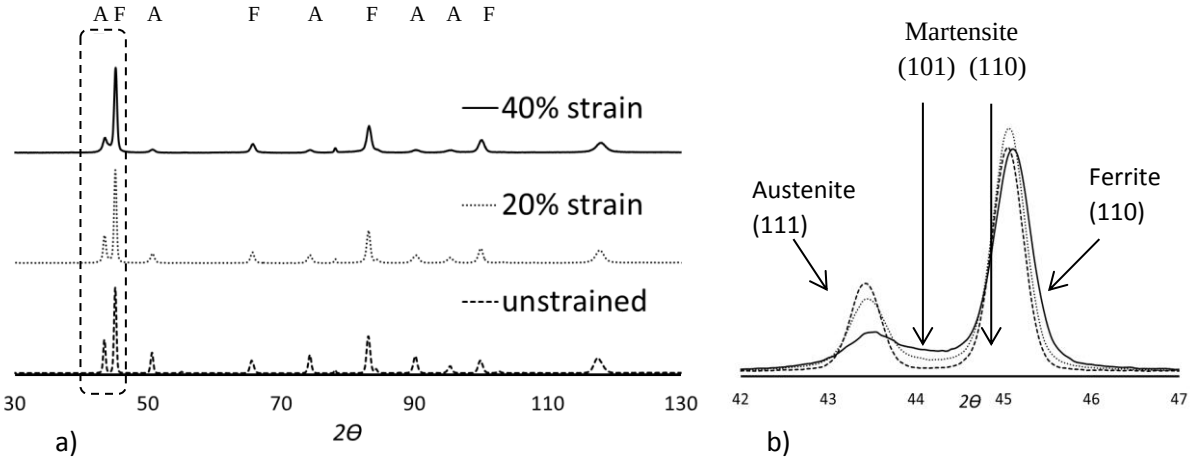

Figure 2a and b. Neutron diffraction pattern of ADI samples, austempered at 350°C and deformed to different strain levels. An enlarged view of the diffraction pattern between 2θ= 42° ~ 47° is shown on the right side. Austenite and ferrite reflections are marked with A and F.

Figures 3 and 4 show the texture evolution of ADI samples (T_γ = 900°C / T_{Aus} = 350°C) with increasing strain. The inverse pole figures have been calculated from measured austenite (111), (200) and ferrite (110), (200) pole figures. The results indicate a weak fibre texture for all samples. Here the typical compression component for austenite [110] (*fcc*) and ferrite [111] (*bcc*) can be readily identified [17]. Comparing the ODFs in figure 4 to the standard ODF of *bcc* and *fcc* materials [18], the texture formation of austenite and ferrite in ADI during the compressive deformation will be identified as follows. The strongest components of austenite phase in the compressed sample are α-fiber // LD spread from (001) [$1\bar{1}0$] to (110) [$1\bar{1}0$] plus (111) [$0\bar{1}1$] and (001) [$\bar{1}\bar{1}0$]. In ferrite the compressive deformation leads to the formation of a texture characterized by two distinct components: (110) [$1\bar{1}2$] Brass and (112) [$11\bar{1}$] Copper.

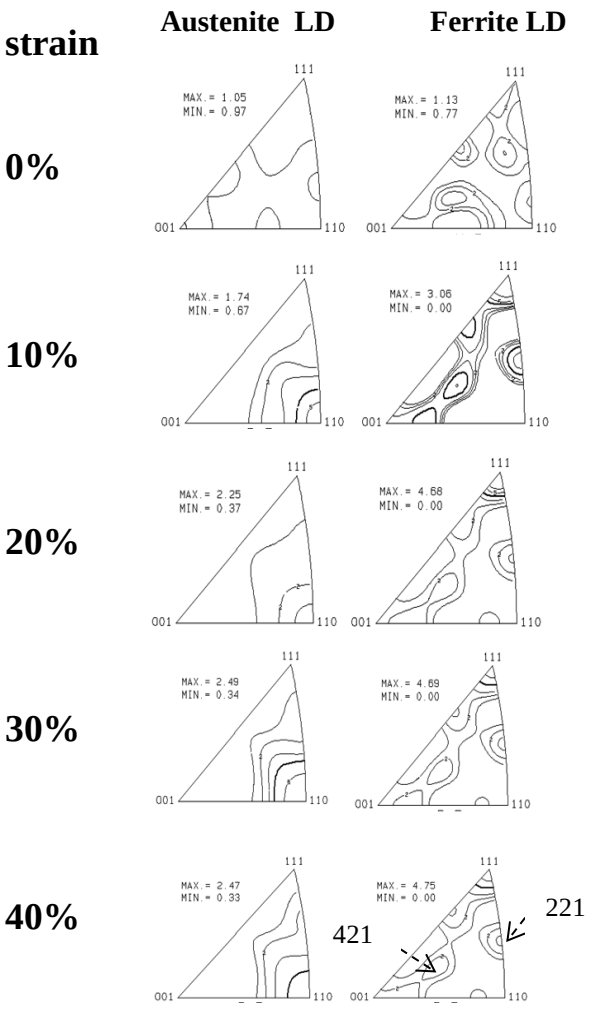

Figure 3. Inverse pole figures of austenite and ferrite phases in ADI (austempered at 350°C) for different strain levels up to 40%.

Comparison of the main texture components - austenite [110] (*fcc*) and ferrite [111] (*bcc*) - of all the differently treated samples (table 1) shows that the texture formation depends only on plastic strains and not on heat treatment conditions. The texture evolution, illustrated by the changes in multiples of random distribution (m.r.d) in the inverse pole figures of the austenite [110] and ferrite [111] directions, which are parallel to the main deformation direction during plastic deformation is shown in figure 5. There is a strong increase in texture during compressive deformation until 20% strain. After reaching 20% strain there is almost no increase with further plastic deformation. This might be attributed to limited activation of dislocation glide systems in *fcc* and *bcc* metals at room temperature. On the other hand the average particle size of austenite and ferrite grains in ADI is in the order of 50 nm [1], nano-crystal sized grain rotation and grain boundary sliding [19] probably take place instead of dislocation gliding during the plastic deformation.

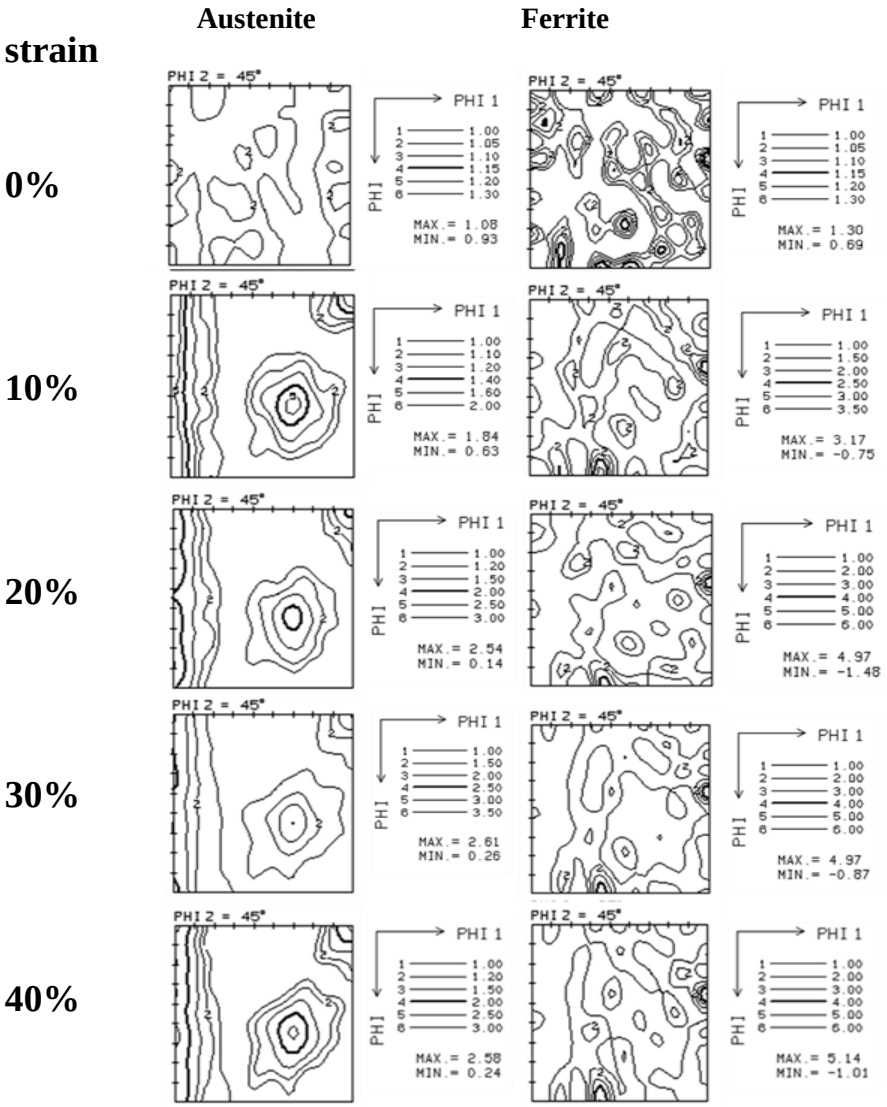

Figure 4. ODFs of austenite and ferrite phases in ADI (austempered at 350°C) for different strain levels up to 40%.

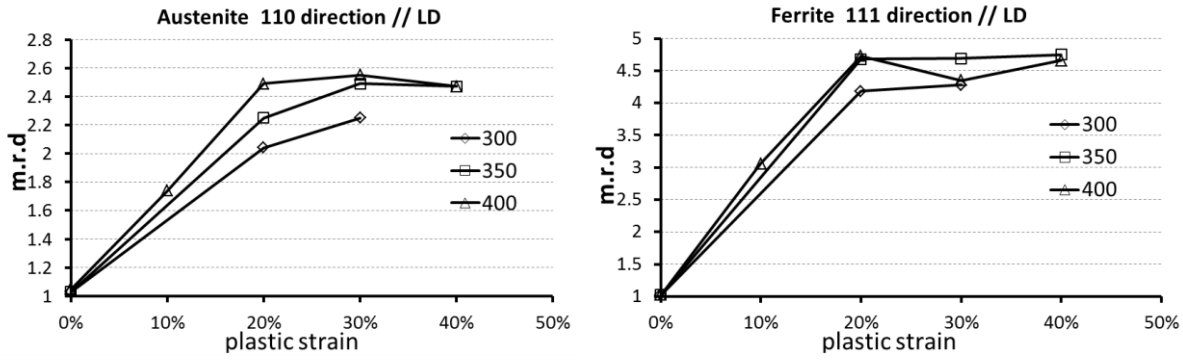

Figure 5. Texture evolution of ADI samples austempered at 300°C, 350°C and 400°C parallel to the main deformation direction during plastic deformation.

3.2 Combining texture and diffraction data for phase analysis

Closer inspection of the inverse pole figures of ferrite reveals additional weak components in [221] and [421] directions (marked in figure 3). These components are usually not found in *bcc* metals (table 2, [18]). Due to the strong overlap of martensite and ferrite reflection positions, intensities for the pole figures cannot be extracted separately and thus these additional components arise most likely from the martensitic phase.

Furthermore this makes it difficult to use the texture results directly when using the ODFs calculated from the (110) and (200) pole figures of ferrite as input in the Rietveld analysis with MAUD. A way around this is to use a single reflection pole figure for the ODF calculation. This is an admissible approach because of the high symmetry of *bcc* crystal structure of ferrite. In addition, originating from the compression deformation martensite as well as ferrite have a distinct orientation relation with the austenite phase. This has been found in most iron based alloys [20-23]. Here the *bcc* ferrite, *bct* martensite and *fcc* austenite are often observed to have a Kurdjumov-Sachs (K-S) and Nishiyama-Wassermann (N-W) orientation relationship. The K-S relation is defined as $(111)\gamma$ // $(110)\alpha$, $[1\bar{1}0]\gamma$ // $[1\bar{1}1]\alpha$, while the N-W relation as $(111)\gamma$ // $(110)\alpha$, $[\bar{1}01]\gamma$ // $[001]\alpha$.

In our case using the (200) pole figure alone yields an ODF and recalculated inverse pole figure in accordance with the standard texture orientations of *bcc* metals (Table 2). As an example figure 6 shows the corresponding ODF and recalculated inverse pole figure for a sample (T_γ = 900°C/ T_{Aus} = 350°C) compressed to 40% strain.

Table 2. Texture orientation // RD or LD in *bcc* and *fcc* metals after different plastic deformation [17].

Cystal structure	tension	compression	rolling
bcc	**[110]**	**[111] and [100]**	**Mainly from (001)[$\bar{1}$ 10] to (111)[$\bar{1}$10]** **Weak component spread from (112)[$\bar{1}$10] to (111)[$\bar{2}$11]**
fcc	**[111]** **[100]**	**Strong component around [110], spread from [110] to [113], plus a weak component [100]**	**Copper-type (123)[$\bar{4}\bar{1}$2]+(146)[$\bar{2}\bar{1}$1]** **Silver-type (110)[$\bar{1}$12]**

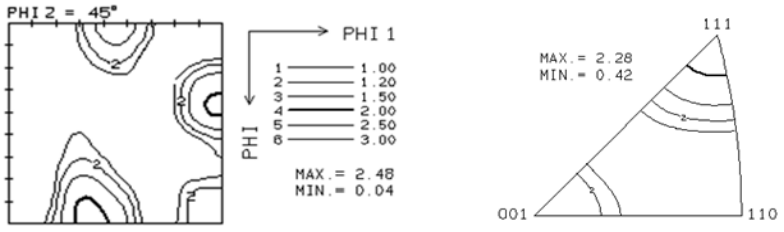

Figure 6. ODF calculated from single component ferrite (200) pole figure of an ADI sample austempered at 350°C and compressed to strain level 40% (left). Corresponding recalculated inverse pole figure (right). Note the absence of the components for the [421] and [221] directions.

3.3 Strain induced martensite transformation

Figure 7 and 8 show the martensite phase fractions in deformed ADI extracted using the recalculated ODFs as input in the Rietveld refinements of the lattice constants, peak shape parameters and phase contents. The strain induced martensite transformation in ADI during plastic deformation is not proportional to the retained austenite content at the beginning of plastic deformation. For the sample treated with T_{Aus} = 400°C and also similar T_{Aus} = 350°C a linear dependence of the martensite phase content with strain is found. Thus at each strain level the same amount of martensite is formed regardless of the initial retained austenite content. However, at around 20% plastic strain the increase in martensite phase fraction deviates from a linear behavior in the sample with the lowest austempering temperature T_{Aus} = 300°C leveling out to about 20% martensite at 40% plastic strain. At this point about 80% of the retained austenite is transformed to marteniste in this sample. To visualize this effect in figure 8 the martensite phase fractions are normalized to the initial retained austenite content from table 1. This shows clearer the dependence on heat treatment parameters, with the highest amount of transformation for the lowest austempering temperature (figure 8). Figure 8 shows that at 40% compressive deformation a total amount of 65% to 80% retained austenite transformed into martensite. Due to sample breakage higher strain levels cannot be achieved using compression and further experiments allowing a higher degree of deformation, for instance cold rolling, are needed to clarify whether the trend seen in the sample austempered at T_{Aus}=300°C becomes apparent in samples heat treated at higher temperatures.

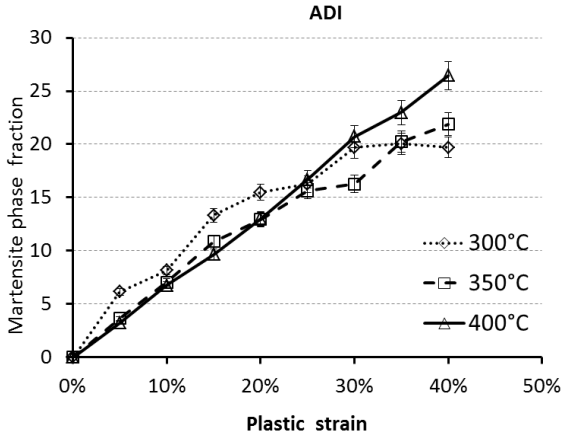

Figure 7. Martensite phase fraction in ADI (austempered at 300°C, 350°C and 400°C) after compressive deformation vs. plastic strain.

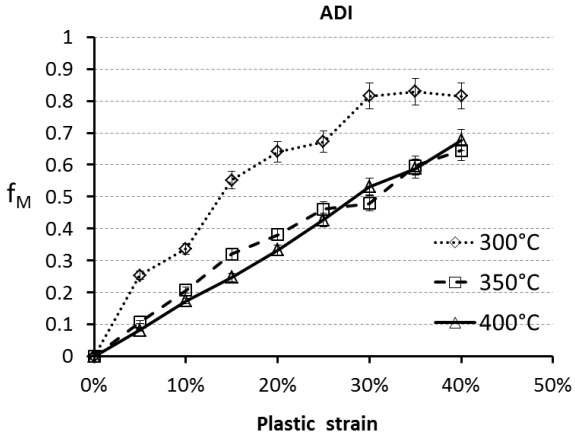

Figure 8. Normalized martensitic phase fraction f_M in ADI after compressive deformation vs. plastic strain.

4. Conclusion

Combining texture information and Rietveld refinements of neutron powder diffraction patterns allows extracting quantitatively phase fractions in ADI. In case of severe overlap of Bragg reflections between marteniste and ferrite in ADI it could be shown that an approach to derive the orientation distribution function for the ferrite phase from just one complete pole figure leads to a more accurate input into the refinement procedure for phase analysis. The results of the quantitative analysis of the martensite phase fractions as a function of deformation shows a dependence of transformation rates with heat treatment parameters with up to 80% of the retained austenite being transformed to martensite for samples heat treated at T_{Aus} = 300°C.

5. References

[1] L Meier, M Hofmann, P Saal, W Volk and H Hoffmann 2013 *Mater. Char.* **85** 124-133
[2] M Daber, P Prasad Rao 2008 *J. Mat. Sci.* **43** 357-367
[3] G Bordin, G C Cecchi and G B Fratucello 1981 *IL Nuovo Cimento* **61B**, N.2
[4] C-H Hsu and T-L Chuang 2001 *Metallurgical and Materials Transactions* A **32A** 2509-2514
[5] J Aranzabal, I Gutierrez, J M Rodriguez-Ibabe and J J Urcola 1997 *Metallurgical and Materials Transactions* A **28A** 1143-1156
[6] S Daber, K S Ravishankar and P Prasad Rao 2008 *J. Mater Sci* **43** 4929-4937
[7] M R Berrahmoune, S Berveiller, K Inal, A Moulin and E Patoor 2004 *Mat.Sci.and Eng.* A **378** 304-307
[8] O Grässel, L Krüger, G Frommeyer and L W Meyer 2000 *Inter. Journal of Plasticity* **16** 1391-1409
[9] W J Dan, S H Li, W G Zhang and Z Q Lin 2008 *Materials and Design* **29** 604-612
[10] M Järvinen 1993 *J. Appl. Cryst.* **26** 525-531
[11] L Lutterotti, S Matthies, H-R Wenk, A J Schultz and J Richardson 1997 *J. Appl. Phys.* **81** 594-600
[12] M Ferrari and L Lutterotti 1994 *J. Appl. Phys.* **76** (11) 7246-55
[13] P Saal, L Meier, X H Li, M Hofmann, M Hoelzel, J N Wagner and W Volk 2015 *Metallurgical Trans.* A, in print
[14] M Hoelzel, A Senyshyn, N Juenke, H Boysen, W Schmahl and H Fuess 2012 *Nucl. Instrum.Meth.* **A667** 32
[15] M Hofmann, G A Seidl, J Rebelo-Kornmeier, U Garbe, R Schneider, R C Wimpory, U Waswuth and U Noster 2006 *Mat. Sci. Forum* **524-525** 211-216
[16] M Dahms and H J Bunge 1989 *J. Appl. Cryst*. **22** 439-447
[17] Hsun Hu 1974 *Texture*, **1** 233-258
[18] U F Kocks, C N Tome and H-R Wenk 2000 *Texture and Anisotropy* (Cambridge University Press)
[19] H van Swygenhoven and Peter Derlet 2001 *Phys. Rev.* **64** 224105
[20] P R Howell, J V Bee and R W K Honeycombe 1979 *Metallurgical Trans.* A, **10A** 1213-1222
[21] G J Mahon, J M Howe and S Mahajan 1989 *Philosophical Magazine Letters*, **59** 273-279
[22] Pat L Mangonon, JR and Gareth Thomas 1970 *Metallurgical Trans.***1** 1577-1586
[23] K Verbecken, L Barbé and D Raabe 2009 *ISIJ International*, **49** 1601-160